Temperature-Dependent Structure of the E·S Complex of *Bacillus stearothermophilus* Alcohol Dehydrogenase†

Xiaohua Zhang and Thomas C. Bruice*

Department of Chemistry and Biochemistry, University of California, Santa Barbara, California 93106

Received October 10, 2006; Revised Manuscript Received November 15, 2006

ABSTRACT: The catalytic chemistry of the thermophilic *Bacillus stearothermophilus* alcohol dehydrogenase (HtADH) closely resembles that of mesophilic horse liver alcohol dehydrogenase (HLADH). Molecular dynamics (MD) simulations of the htADH·NAD^+·EtO^- complex at 298, 323, and 348 K show that the structure of the ligated Zn^{2+}···EtO^- complex varies slightly with change in temperature. The MD-created Boltzmann distribution of htADH·NAD^+·EtO^- structures establishes the formation of multiple states which increase in number with a decrease in temperature. The motions of the cofactor domain are highly correlated with the motions of NAD^+ at the optimal growth temperature (348 K), with NAD^+ being pushed toward the substrate by Val260. With a decrease in temperature, the motion together of the cofactor and substrate is reversed, and at 298 K, the nicotinamide ring of the cofactor moves away from the substrate. Both the distance between and the angle of approach of C4 of NAD^+ and H_D of EtO^- become distorted from those of the reactive conformation. The percentages of ground state present as the reactive conformation at different temperatures are approximately correlated with the k_{cat} for the htADH enzymatic reaction. The rate constant for the htADH·NAD^+·EtOH → htADH·NAD^+·EtO^- proton dissociation, which is mediated by Thr40−OH, becomes slower at lower temperatures. The time-dependent distance between EtO^- and Thr40−OH reveals that the Thr40 hydroxyl group sways between the substrate and NAD^+ ribose 2′-hydroxyl group at the optimal enzyme growth temperature, and this movement is effectively frozen out as the temperature decreases. The temperature dependence of active site conformations is due to the change in both long-range and short-range motions of the E·S complex.

The thermophilic *Bacillus stearothermophilus* alcohol dehydrogenase (htADH)[1] is a homotetrameric enzyme. Each monomer comprises 339 amino acid residues, a catalytic zinc ion, a structural zinc ion, and a NAD^+ cofactor (*1*). The monomer folds into a tertiary structure with two functionally different domains: cofactor-binding domain (residues 150−285) and catalytic domain (residues 1−149 and 286−339). The cofactor-binding pocket and substrate-binding pocket are formed within the interstices between the two domains. The structure of the htADH E·S complex is homologous to that of *Escherichia coli* ADH and very similar to that of dimeric mesophilic horse liver alcohol dehydrogenase. The htADH enzymatic reaction has been shown to occur in two steps (*2*−*4*) (Figure 1). The (a) htADH·NAD^+·RCH_2OH → htADH·NAD^+·RCH_2O^- + H^+ and (b) htADH·NAD^+·RCH_2O^- → htADH·NADH·RCHO reactions are depicted in Chart 1. Both ribose and nicotinamide portions of the cofactor are reactants in the proton transfer and following hydride equivalent transfer, respectively. Thus, positioning of the entire cofactor is critical to the enzymatic reaction.

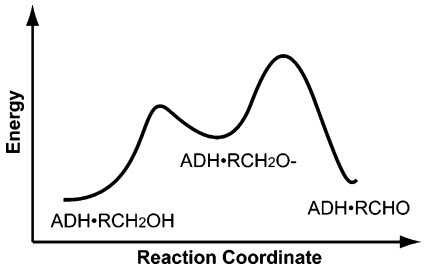

FIGURE 1: Energy profile for the ADH enzymatic reaction.

Accumulated experimental evidence supports a role for quantum tunneling in hydride equivalent transfers (*5*−*7*), and much of the theoretical attention has been given to calculations of the energy or free energy of the mesophilic horse liver alcohol dehydrogenase reaction (*8*−*11*). Recent kinetic isotopic studies of htADH support a thermally induced enzyme dynamic contribution to such quantum tunneling (*12*−*15*). Our previous studies of horse liver alcohol dehydrogenase (*16*) have demonstrated that both the active ground state conformation of the E·S complex and the anticorrelated motions of the enzyme facilitate proton and hydride equivalent transfer (*17*−*19*). This study has been directed toward the temperature dependence of the structure and motions of the htADH·NAD^+·EtO^- ground state.

The Arrhenius plots of rate constants for the oxidation of benzyl alcohol by htADH exhibit steeper slopes at reduced temperatures (*12*). Evidence of tunneling at elevated temperatures was a deviation from the semiclassical Swain−

† Supported by National Institutes of Health Grant 5R37DK9174-43.

* To whom correspondence should be addressed. Telephone: (805) 893-2044. Fax: (805) 893-2229. E-mail: tcbruice@chem.ucsb.edu.

[1] Abbreviations: ADH, alcohol dehydrogenase; htADH, *Bacillus stearothermophilus* alcohol dehydrogenase; NAD^+, nicotinamide adenine dinucleotide; MD, molecular dynamics; KIE, kinetic isotopic effect.

10.1021/bi062110+ CCC: $37.00
Published on Web 12/29/2006

Chart 1

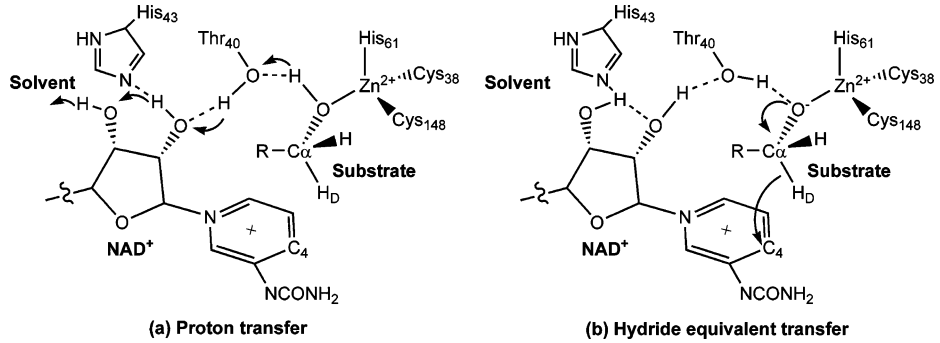

Schaad relationship measured for hydrogen−deuterium (H−D) kinetic isotopic effects (KIEs) using the mixed labeling experiment (*12*, *20*, *21*). A temperature-dependent H−D exchange study has revealed that the htADH system undergoes transitions with temperature, which results in a more dynamic conformation at higher temperatures (*22*). Such a phenomenon of temperature-dependent enzyme activity has been previously observed in several different types of thermophilic enzymes (*23*−*25*). Most recently, we have employed molecular dynamics (MD) simulations in examining the temperature dependence of the E·S complexes of *Sulfolobus sulfataricus* thermophilic indole-3-glycerol phosphate synthase and *Thermus thermophilus* chorismate mutase (*26*−*28*).

METHODS

The starting structure of the htADH·NAD^+·EtO^- intermediate was optimized from the X-ray crystallography structure (PDB entry 1RJW) by Ceccarelli et al. (*1*) after the substrate analogue trifluoroethanol (TFE) was replaced in the X-ray structure with EtO^-. The CHARMM27 force field was employed in the MD simulations (*29*). The electrostatic potential of EtO^- at the B3LYP/6-311+G(2d, p) level was obtained from the optimized geometry of EtO^- using the Merz−Kollman scheme (*30*) implemented in Gaussian03 (*31*). The parameters for EtO^- were optimized until the CHARMM results and ab initio data were in a good agreement (*32*). For the cysteine thiolate (Cys-S^-), the force field was chosen in a manner suggested by Nilsson et al. (*33*).

The htADH·NAD^+·EtO^- complex was solvated using a water sphere with a radius of 42 Å, centered at one of the catalytic zinc ions. Water molecules within 2.8 Å of any non-hydrogen enzyme·cofactor·substrate atoms were removed. Energy minimization was carried out to remove the unfavorable interactions between the solute and solvent. Voids generated after brief Langevin dynamics were filled with water molecules so that the solvent density was correct. The resulting system contained 6653 TIP3P water molecules (*34*). Stochastic boundary conditions were applied to the system (*35*). The residues more than 42 Å (r) from the center of the water sphere were fixed in the simulations. The region in which r < 40 Å was selected as the reaction zone; the region in which 40 Å < r < 42 Å was selected as the buffer zone, and the region in which r > 42 Å was selected as the reservoir zone. The atoms in the reaction zone were treated with Newtonian dynamics, while atoms in the buffer zone were restrained by harmonic constraints and simulated using Langevin dynamics. The friction constants used in the integration of the Langevin equation were 250 and 62 ps^{-1} for the protein atoms and water molecules, respectively. A spherical boundary potential centered at the origin of the water cap was employed to maintain the correct average distribution of water molecules (*36*, *37*). The SHAKE algorithm (*38*) was applied to fix the covalent bonds involving hydrogen. Then, energy minimizations were performed using the steepest descent (SD) and adopted basis Newton−Raphson (ABNR) algorithms. The MD simulations with a time step of 1 fs for the integration of the equations of motion were carried out at three different temperatures, 298, 323, and 348 K. The distances between residues in the cofactor-binding pocket, substrate, and cofactor were constrained with the harmonic forces at the beginning of MD simulations and released steadily at equilibrium stage. Each trajectory was followed to 5 ns after equilibrium.

Motions of NAD^+ and the htADH enzyme were determined by the cross-correlation motion analysis of the MD trajectories (*39*). Cross-correlated motion analysis is capable of revealing the long-range (usually a time period of nanoseconds) motions of the enzyme (*40*). The correlated coefficients between NAD^+ and the htADH residues were calculated by eq 1:

$$C_i = \langle \Delta\vec{r}_i \cdot \Delta\vec{r}_{NAD^+} \rangle / (\langle \Delta\vec{r}_i^{\,2} \rangle \langle \Delta\vec{r}_{NAD^+}^{\,2} \rangle)^{1/2} \qquad (1)$$

where Δr_i is the average coordinate displacement of htADH residue i from the mean position and Δr_{NAD^+} is that for NAD^+. The correlated coefficient ranges from −1.0 to 1.0. Correlated (postive) residues move in the same direction as NAD^+, and anticorrelated (negative) residues move in the opposite direction. A completely correlated or anticorrelated motion (correlation coefficients, $C_i = 1$ or $C_i = -1$) denotes that the motions have the same or opposite phase and period.

RESULTS

The correlated coefficients between the htADH residues and NAD^+ at 298 and 348 K were calculated from 5 ns MD trajectories (Figure S1 of the Supporting Information). Positively correlated coefficients denote that the motions of the htADH residues and NAD^+ are in the same direction, while negative ones designate that they move in opposite directions. The major portions of the cofactor-binding domain are positively correlated with NAD^+ at both 298 and 348 K. However, a difference is revealed as the correlated coefficients between the cofactor-binding domain and NAD^+ are averaged (0.31 and 0.50 at 298 and 348 K, respectively).

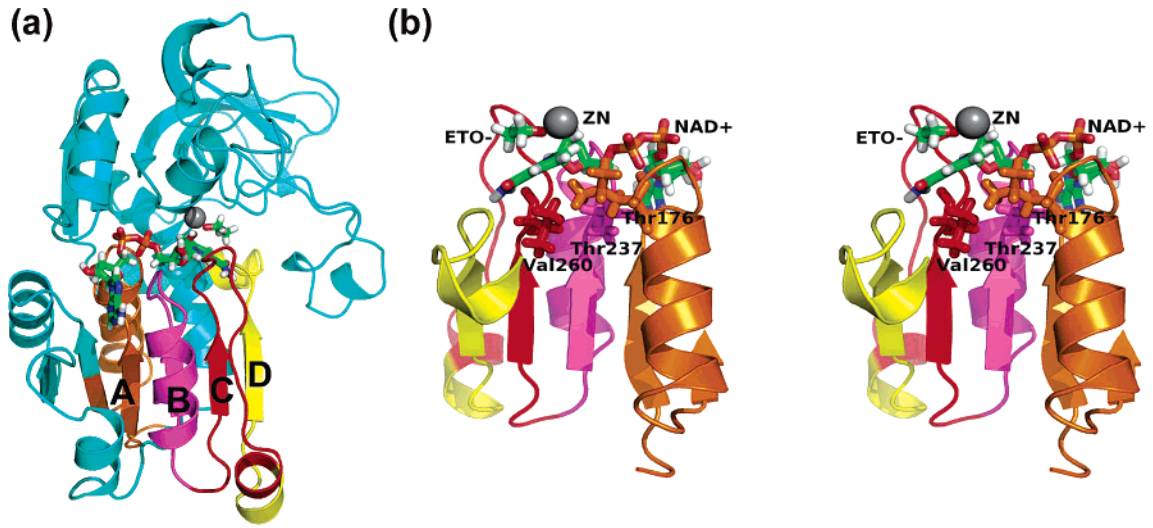

FIGURE 2: (a) Plot of correlated motions mapped onto the htADH monomer. The htADH enzyme is represented with ribbons. NAD^+ and the substrate are represented with sticks. The Zn^{2+} ion is represented with a sphere. Only the crucial correlated coefficients between NAD^+ and htADH were mapped. Four crucial fragments of the htADH enzyme have been labeled in different colors: orange for fragment A (residues 161−190), magenta for fragment B (residues 231−250), red for fragment C (residues 251−273), and yellow for fragment D (residues 273−290). Fragments A−D are correlated to each other. The cofactor domain is anticorrelated to the catalytic domain. The averages of correlated coefficients for fragments A−D are 0.37, 0.35, 0.17, and 0.16 at 298 K and 0.55, 0.57, 0.42, and 0.46 at 348 K, respectively. (b) Stereoview of fragments A−D. Three residues, Leu176, Thr237, and Val260 in fragments A−C, respectively, are represented with sticks. The correlation coefficients between these three residues and NAD^+ at 298 and 348 K are different (0.72 and 0.83 for Leu176, 0.40 and 0.80 for Thr237, and 0.56 and 0.80 for Val260).

This indicates the motions of the cofactor-binding domain are better correlated with that of NAD^+ at higher temperatures.

The correlated coefficients between NAD^+ and htADH were mapped for fragments A−D which constitute the cofactor-binding domain (Figure 2). The averages of correlated coefficients for fragments A−D are significantly larger at 348 K than that at 298 K. Fragment C is of primary interest because it is adjacent to the nicotinamide ring of NAD^+. Fragment C is only slightly correlated with the motions of NAD^+ at 298 K. However, the correlated motion is significant at 348 K. In particular, Val260 in fragment C, which is the equivalent of Val203 in horse liver ADH (*3*), is in van der Waals contact with the nicotinamide ring. The motion of Val260 is well-correlated with that of NAD^+ at the optimal growth temperature. The temperature dependence of correlated motions for Thr237 is much the same as that of Val260. The correlated coefficient for Leu176 increases only slightly, suggesting that the motion of Leu176 is rarely affected by the temperature. Fragment D is located at the bottom of the cofactor-binding pocket and connects the cofactor-binding domain to the catalytic domain. NAD^+ is loosely bound with the cofactor-binding pocket at 298 K while perfectly bound for catalysis at the optimal growth temperature.

It has been shown with a number of enzymes that k_{cat} is dependent upon the portion of the Boltzmann distribution of the ground state present as reactive conformations (*41*−*43*). Such conformations have been termed near-attack conformations (NACs) (*42*). NAC is geometrically defined by both a van der Waals distance of two reacting atoms and their approaching angle. The NAC of the htADH hydride equivalent transfer reaction is defined in Figure 3. The van der Waals distance between H_D and C4 is <3.0 Å. The approaching angle of H_D with respect to the C4 atom of the nicotinamide ring [$\angle C\alpha-H_D\cdots C4$ (θ)] is larger than 132° but less than 180° (*17*).

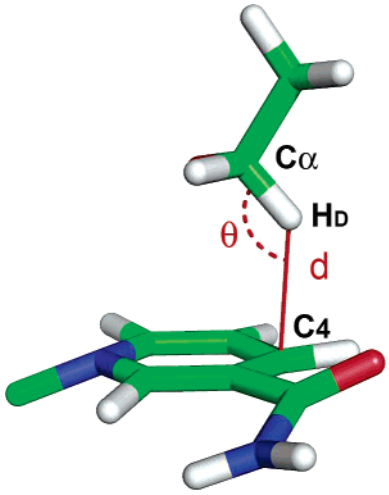

FIGURE 3: Definition of NAC for the htADH hydride equivalent transfer. In the NAC structure, transfer distance d (H_D-C4) ≤ 3.0 Å and approaching angle θ ($\angle C\alpha-H_D\cdots C4$) is larger than 132° but less than 180°.

Obtained from long-term MD simulations, plots of hydride equivalent transfer distance (d) versus approaching angle (θ) provide the Boltzmann distribution of ground state conformations of the htADH·NAD^+·EtO^- intermediate at different temperatures (Figure 4). The distribution of d versus θ is approximately reciprocal: a larger d is associated with a smaller θ. Plots at lower temperatures (298 and 323 K) have shown that the E·S structure exists as three distinguishable states: state 1 at the bottom right-hand region, state 3 at the top left-hand region of the plots, and state 2 between states 1 and 3 (Figure 4b,c). The average H_D-C4 distances (d) of state 1 at 298 and 323 K are 2.78 ± 0.23 and 2.61 ± 0.27

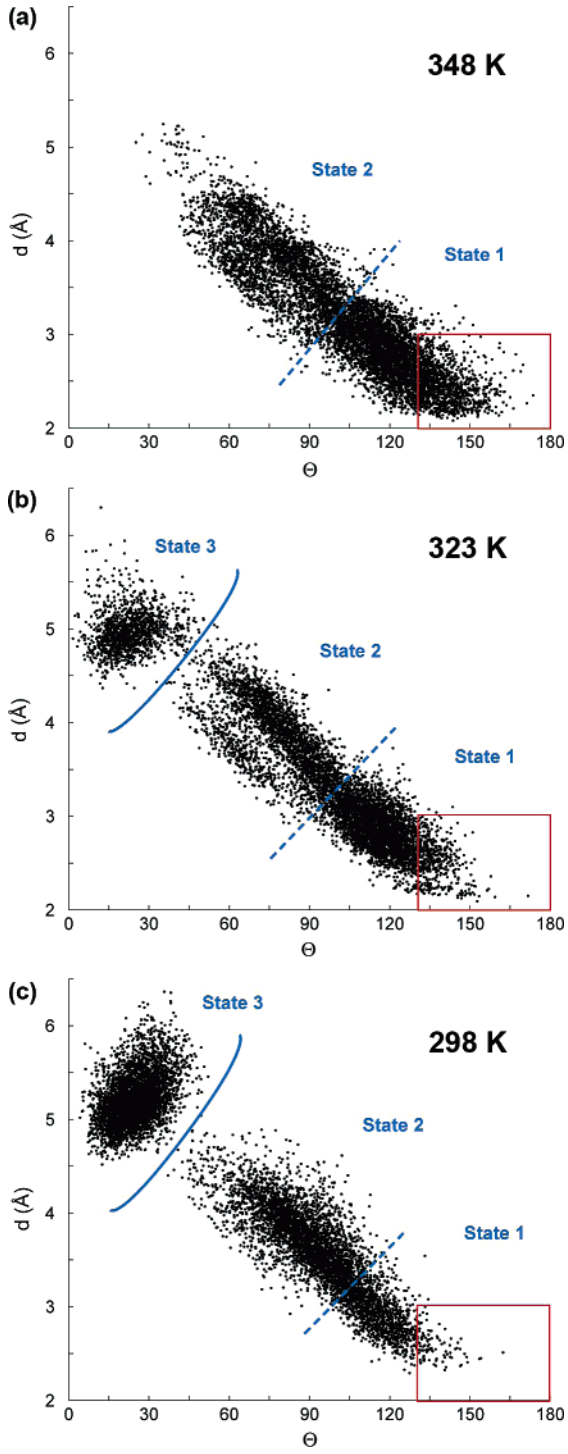

FIGURE 4: Plot of the hydride equivalent transfer distance (d) vs the approaching angle (θ) obtained from the stable dynamic run (4 ns) at three different temperatures (298, 323, and 348 K). The distribution has been divided into three portions for 298 and 323 K and two portions for 348 K. They are labeled as states 1−3. A total of 8000 ground state conformations are included, and NAC structures are enclosed in the red box in the bottom right-hand corner.

Å, respectively. The average of d in state 3 at 298 K is 5.20 ± 0.28 Å, while that at 323 K is 4.92 ± 0.19 Å. The large average value of d in state 3 at 298 K indicates that the cofactor-binding pocket is enlarged as the temperature is lowered. There are 44% of the total conformations present in state 3 at 298 K while only 16% in state 3 at 323 K. At the optimal growth temperature (348 K), state 3 has vanished (Figure 4a). The average values of d are 3.77, 4.02, and 4.29 Å at 348, 323, and 298 K, respectively, while the average values of θ are 112°, 92°, and 86°, respectively. The region where NAC occurs is located in state 1 and is within the red box in Figure 4. The percentages of ground state present as the reactive conformer are 24%, 4%, and 0.6% at 348, 323, and 298 K, respectively. The NAC population becomes smaller as the temperature decreases. The k_{cat} values of the htADH enzymatic reaction are ∼37 and ∼300 s^{-1} at 298 and 323 K, respectively (*12*). From 323 to 298 K, the percentage of ground state present as NAC decreases by 7-fold, which is comparable to the ratio of k_{cat} at two temperatures (8-fold).

Snapshots of states 1 and 3 extracted from the MD trajectories are presented in stereoview (Figure 5). The hydride equivalent transfer distance between H_D and C4 is primarily determined by the relative position of the Zn^{2+} catalytic site and the NAD^+ cofactor. The conformation of the NAD^+ cofactor is largely determined by the cofactor domain. As shown in Figure 5, the three residues within van der Waals contact of the NAD^+ cofactor are Leu176, Thr237, and Val260. They are included in fragments A−C, respectively, as described. The distances between CD1 of residue Leu176 and C5 of NAD^+ are 3.55 and 4.06 Å in states 1 and 3, respectively. Those for Thr237 (CG2) and NAD^+ (O4′) are 3.64 and 3.81 Å, respectively. Larger distances in state 3 indicate weaker interactions between NAD^+ and Leu176, as do NAD^+ and Thr237.

The amide group of Val260 forms a stable hydrogen bond with the amide group of nicotinamide, and the hydrophobic side chain of Val260 is in contact with the C2 atom of the nicotinamide ring. A major difference between the two conformations of nicotinamide from states 1 and 3 is in the dihedral angles, χ_1 (N7−C7−C3−C2) and χ_2 (H71−N7−C7−C3) (Chart 2). χ_1 is 17° and 28° and χ_2 3° and 16° for states 1 and 2, respectively. This difference is due to the nicotinamide ring being pushed toward the ligated EtO^-. The pushing motion is expressed through the hydrogen bond between the Val260 amide group and the nicotinamide amide group, as well as the Val260 side chain which is within van der Waals distance of the nicotinamide ring. State 3 is created by expanding the cofactor-binding pocket at lower temperatures. This expansion changes the distance between the CG1 atom of Val260 and the C2 atom of the nicotinamide ring from 3.71 to 4.30 Å. Simultaneously, the hydrogen bond between the 2′-ribose hydroxyl group of NAD^+ and the hydroxyl group of Thr40 present in state 1 is disrupted in state 3. As the nicotinamide ring moves away, the interstice between nicotinamide and the Zn^{2+} catalytic site becomes larger. The hydride equivalent transfer distance between H_D of the substrate and C4 of the nicotinamide is expanded from 2.55 to 5.18 Å.

The substrate intermediate (EtO^-) and the three side chain heteroatoms of the residues, Cys38−S^-, Cys138−S^-, and His61 (NE2), are coordinated with the Zn^{2+} ion in a distorted tetrahedral configuration (Figure 5). The partial charge of the cysteine thiolate (Cys-S^-) was set to −0.80 (*33*), and the partial charge of oxygen (O1) in EtO^- is optimized to be −0.91 by a procedure described in Methods. The experimental (*1*) and theoretical distances between the Zn^{2+} ion and side chain heteroatoms and hydroxyl oxygen are in good agreement (Table S1 of the Supporting Information).

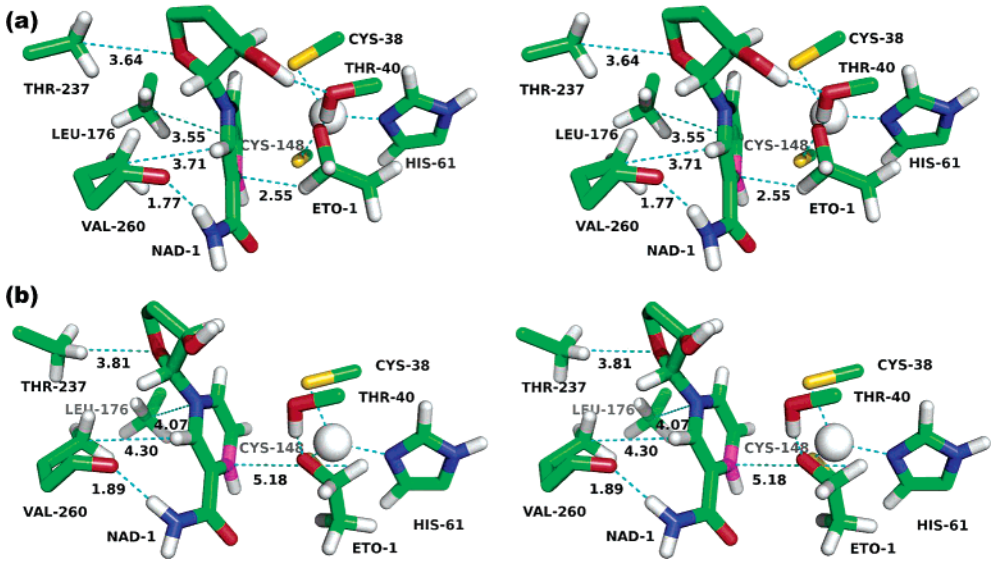

FIGURE 5: Stereoplots of the activity site in two different states. Plot a corresponds to state 1, and plot b corresponds to state 3. Only the essential parts of the residues and cofactor near the Zn^{2+} catalytic site are shown. All the carbon atoms are colored green except C4 which is purple. The oxygen, nitrogen, hydrogen, sulfur, and zinc atoms are colored red, blue, white, yellow, and gray, respectively. The distances for the atoms involved in hydrogen bonds and van der Waals contacts are shown in dashed lines. Some critical distances are labeled with numbers.

Chart 2

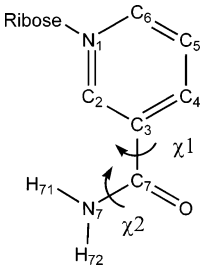

The standard deviations of time-dependent distances between the Zn^{2+} ion and coordinated atoms are all less than 5%, indicating that the coordination distances between the Zn^{2+} ion substrate and neighboring residues are very stable regardless of temperature.

In the starting structure for the MD simulations, the hydroxyl group of Thr40 is hydrogen bonded with the hydroxyl oxygen of EtO^-. The average distance of the heavy atoms involved in the proton transfer (Chart 1a) is shown in Table 1. The average distance from Thr40−OH to EtO^- exhibits an only small fluctuation at 298 K (2.72 ± 0.11 Å) compared to that at higher temperatures (3.40 ± 0.66 and 3.48 ± 0.70 Å at 323 and 348 K, respectively). This suggests that the structure involved in the proton transfer pathway is frozen at low temperatures due to the weaker thermal motions of the htADH enzyme. The temperature-dependent distance from Thr40−OH to EtO^- at 348 K (Figure 6b) reveals a variation between two states at a time period of 1−1.5 ns. As expected, the active site of htADH undergoes more

Table 1: Average Distances among the Heavy Atoms Involved in the Proton Transfer Pathway

	MD at 298 K	MD at 323 K	MD at 348 K
EtO^- (O1)−Thr40 (OG1)	2.72 ± 0.11	3.40 ± 0.66	3.48 ± 0.70
Thr40 (OG1)−NAD^+ (NO2′)	4.01 ± 0.25	3.65 ± 0.71	3.61 ± 0.61
NAD^+ (NO2′)−His43 NE2	3.75 ± 0.27	3.39 ± 0.35	3.35 ± 0.38
His43 (NE2)−NAD^+ (NO3′)	3.00 ± 0.20	3.78 ± 0.41	3.82 ± 0.53

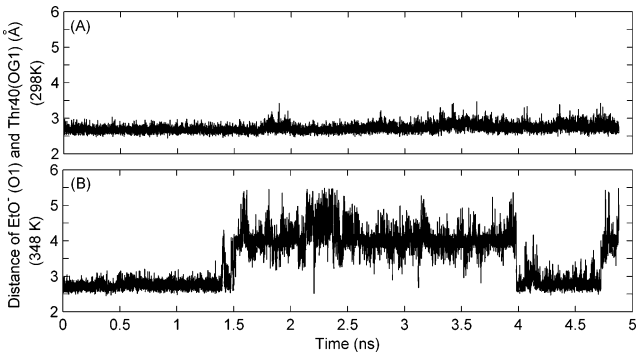

FIGURE 6: Time-dependent distance between the hydroxyl oxygen of EtO^- and that of Thr40−OH obtained from MD simulations at 298 and 348 K.

significant motions at higher temperatures, enabling the hydroxyl group of Thr40 to fluctuate between the substrate and 2′-hydroxyl group of NAD^+ ribose. By doing so, Thr40 is able to facilitate the proton transfer by conveying the proton to solvent (Chart 1).

The hydrogen bond between the imidazole of His43 and the 3′-hydroxyl group of NAD^+ ribose is stable at 298 K, while the imidazole of His43 is hydrogen bound to the 2′-hydroxyl group of NAD^+ ribose at 323 and 348 K. This is due to the enlargement of the interstice between the cofactor-binding domain and catalytic domain at low temperatures. As a consequence, the hydrogen bond between the hydroxyl group of Thr40 and the 2′-hydroxyl group of NAD^+ is disrupted. At 348 K, the 3′-hydroxyl group of NAD^+ ribose is closer to His43 and Thr40 is closer to the substrate. This subtle difference in the structure at different temperatures leads to a pivotal consequence. The placements of heavy atoms along the proton transfer pathway are more equidistant at 323 and 348 K than at 298 K. The abnormal larger distance (>4 Å) between Thr40 (OG1) and NAD^+ (NO2)′ at 298 K must result in an increase in the energy barrier for proton transfer from EtOH.

DISCUSSION

The oxidation of the substrate by htADH involves proton and hydride equivalent transfers (Chart 1). In the studies of horse liver alcohol dehydrogenase, both steps have been considered to be partially or largely facilitated by conformational motions within the active site (*17*, *19*). Short-range local motions are often coupled to longer-range conformational motions (*44*, *45*). In htADH, the thermal motion of the cofactor domain shapes the NAD^+ conformation, allowing it to directly assist both proton and hydride equivalent transfer. The correlated motions between NAD^+ and several constituents of the cofactor domain, such as fragments A−D, are larger at higher temperatures (Figure 2). This is particularly so for fragment C and NAD^+. The distance between the side chain of Val260 and the NAD^+ cofactor is shortened by the cofactor-binding domain motions, resulting in movement of the Val260 side chain toward the NAD^+ and subsequent pushing of the NAD^+ cofactor toward the substrate. The cofactor-binding domain motions are frozen at low temperatures, and Val260 moves away from the nicotinamide of NAD^+. This change is due to the expansion of the cofactor-binding pocket. Thus, the hydride equivalent transfer distance is enlarged.

From the plots of transfer distance versus approaching angle (Figure 4), it can be seen that the htADH·NAD^+·EtO^- complex exists in more than one average conformation (states 1−3). At the optimal growth temperature, the cofactor-binding pocket is tightened by the pushing motions of the cofactor-binding domain. As the temperature decreases, these correlated motions are weakened and the cofactor-binding pocket expands. At 348 K, there are only two overlapping states, 1 and 2, while a nonoverlapping state 3 with a longer transfer distance is present at 323 K. As the temperature continues to decease to 298 K, state 3 predominates.

In our MD simulation of the htADH·NAD^+·EtO^- complex, the percentage of the ground state present as NAC increases by 7-fold from 298 to 348 K. This is comparable to the ratio (∼8-fold) of k_{cat} at 298 and 348 K. From the correlation motion calculation, it has been shown that motions of the htADH cofactor domain are highly correlated to NAD^+ at high temperatures. This leads to the shortening of the reaction coordinate for the hydride equivalent transfer. From both long-range and short-range local motions, htADH regulates the hydride equivalent transfer distance by the correlated motions between NAD^+ and the cofactor domain.

The proton transfer accompanying ionization of EtOH to EtO^- and H^+ in the first step of the alcohol dehydrogenase enzymatic reaction is mediated by the hydroxyl group of Thr40 in htADH (and a serine in horse liver alcohol dehydrogenase). The time-dependent distance has shown that Thr40−OH oscillates in hydrogen bonding between EtO^- and the 2′-hydroxyl group of NAD^+ on a nanosecond time scale at 348 K, while this motion is frozen by a tight hydrogen bond with a substrate at 298 K. This observation is consistent with the suggestion by Klinman and co-workers that that some regions within htADH are less dynamic and demonstrate limited cooperative protein motion at reduced temperatures (*1*, *12*, *22*). At higher temperatures, oscillation of the Thr40 side chain between the substrate and NAD^+ cofactor facilitates the proton transfer. The loss in the flexibility of Thr40 at lower temperatures reduces the rate of the proton shifting along the hydrogen bond network (Chart 1).

The motion of the htADH active site structure is lowered as the temperature is decreased, and the motion of the cofactor domain at low temperatures is less correlated to that of NAD^+, leading to a distorted active site in which the substrate is less likely to reach a reactive conformation.

CONCLUSION

The temperature dependence of the structure of the *B. stearothermophilus* alcohol dehydrogenase E·S complex (htADH·NAD^+·EtO^-) has been investigated by MD simulations at 298, 323, and 348 K. The structure of the E·S complex is affected by both long-range and short-range local motions. The conformation of NAD^+ is largely determined by the motions of the cofactor domain, and the motions of NAD^+ are well correlated to the cofactor domain at the optimal growth temperature but not at low temperatures. The correlated motions are crucial to a favorable Boltzmann distribution of reactive conformations of the htADH·NAD^+·EtO^- complex. Multiple states were found from plots of d versus θ. State 3, which corresponds to the larger transfer distance, is not present at the optimal growth temperature. At 348 K, the nicotinamide ring of NAD^+ is pushed toward the substrate to form a perfect conformation (NAC) in which the C4 atom of nicotinamide and the H_D atom of substrate are brought together within van der Waals distance and the approaching angle is appropriate for the reaction. Furthermore, the nicotinamide ring moves away from the substrate with a hydrogen bond between the NAD^+ amide group and Val260 residue amide group at lower temperatures. As the temperature is lowered and the enzyme motions are frozen, the side chain of Thr40 sticks to the substrate instead of oscillating between the substrate and 2′-hydroxyl group of the NAD^+ ribose, preventing the $EtOH \rightarrow EtO^- + H^+$ reaction. Thus, both proton and hydride equivalent transfer in the alcohol dehydrogenase enzymatic reaction are modulated by the correlated motions between NAD^+ and the cofactor domain.

ACKNOWLEDGMENT

We express appreciation to the National Partnership for Advanced Computational Infrastructure for its generous allocation of computational resources at DataStar at the University of California at San Diego Supercomputing Center (SDSC). We acknowledge Professor Judith P. Klinman's introduction of the enzyme to us and her continued interest. We thank Dr. Luo Jia and Istvan Szabo for helpful discussion. Valuable comments by reviewers are acknowleged.

SUPPORTING INFORMATION AVAILABLE

Stem plots of correlation coefficients between htADH and NAD^+ at 298 and 348 K (Figure S1) and average distances between the catalytic Zn^{2+} ion and heteroatoms of coordinated residues and/or substrates (Table S1). This material is available free of charge via the Internet at http://pubs.acs.org.

REFERENCES

1. Ceccarelli, C., Liang, Z. X., Strickler, M., Prehna, G., Goldstein, B. M., Klinman, J. P., and Bahnson, B. J. (2004) Crystal structure

and amide H/D exchange of binary complexes of alcohol dehydrogenase from *Bacillus stearothermophilus*: Insight into thermostability and cofactor binding, *Biochemistry 43*, 5266−5277.
2. Bahnson, B. J., Park, D. H., Kim, K., Plapp, B. V., and Klinman, J. P. (1993) Unmasking of Hydrogen Tunneling in the Horse Liver Alcohol-Dehydrogenase Reaction by Site-Directed Mutagenesis, *Biochemistry 32*, 5503−5507.
3. Bahnson, B. J., Colby, T. D., Chin, J. K., Goldstein, B. M., and Klinman, J. P. (1997) A link between protein structure and enzyme catalyzed hydrogen tunneling, *Proc. Natl. Acad. Sci. U.S.A. 94*, 12797−12802.
4. Rubach, J. K., and Plapp, B. V. (2003) Amino acid residues in the nicotinamide binding site contribute to catalysis by horse liver alcohol dehydrogenase, *Biochemistry 42*, 2907−2915.
5. Nagel, Z. D., and Klinman, J. P. (2006) Tunneling and dynamics in enzymatic hydride transfer, *Chem. Rev. 106*, 3095−3118.
6. Kohen, A., and Klinman, J. P. (1998) Enzyme catalysis: Beyond classical paradigms, *Acc. Chem. Res. 31*, 397−404.
7. Benkovic, S. J., and Hammes-Schiffer, S. (2003) A perspective on enzyme catalysis, *Science 301*, 1196−1202.
8. Alhambra, C., Corchado, J. C., Sanchez, M. L., Gao, J. L., and Truhlar, D. G. (2000) Quantum dynamics of hydride transfer in enzyme catalysis, *J. Am. Chem. Soc. 122*, 8197−8203.
9. Antoniou, D., and Schwartz, S. D. (2001) Internal enzyme motions as a source of catalytic activity: Rate-promoting vibrations and hydrogen tunneling, *J. Phys. Chem. B 105*, 5553−5558.
10. Billeter, S. R., Webb, S. P., Agarwal, P. K., Iordanov, T., and Hammes-Schiffer, S. (2001) Hydride transfer in liver alcohol dehydrogenase: Quantum dynamics, kinetic isotope effects, and role of enzyme motion, *J. Am. Chem. Soc. 123*, 11262−11272.
11. Cui, Q., Elstner, M., and Karplus, M. (2002) A theoretical analysis of the proton and hydride transfer in liver alcohol dehydrogenase (LADH), *J. Phys. Chem. B 106*, 2721−2740.
12. Kohen, A., Cannio, R., Bartolucci, S., and Klinman, J. P. (1999) Enzyme dynamics and hydrogen tunnelling in a thermophilic alcohol dehydrogenase, *Nature 399*, 496−499.
13. Rucker, J., and Klinman, J. P. (1999) Computational study of tunneling and coupled motion in alcohol dehydrogenase-catalyzed reactions: Implication for measured hydrogen and carbon isotope effects, *J. Am. Chem. Soc. 121*, 1997−2006.
14. Basner, J. E., and Schwartz, S. D. (2005) How enzyme dynamics helps catalyze a reaction in atomic detail: A transition path sampling study, *J. Am. Chem. Soc. 127*, 13822−13831.
15. Fan, F., and Gadda, G. (2005) Oxygen- and temperature-dependent kinetic isotope effects in choline oxidase: Correlating reversible hydride transfer with environmentally enhanced tunneling, *J. Am. Chem. Soc. 127*, 17954−17961.
16. Ramaswamy, S., Eklund, H., and Plapp, B. V. (1994) Structures of Horse Liver Alcohol-Dehydrogenase Complexed with NAD^+ and Substituted Benzyl Alcohols, *Biochemistry 33*, 5230−5237.
17. Luo, J., and Bruice, T. C. (2001) Dynamic structures of horse liver alcohol dehydrogenase (HLADH): Results of molecular dynamics simulations of HLADH-NAD^+-$PhCH_2OH$, HLADH-NAD^+-$PhCH_2O^-$, and HLADH-NADH-PhCHO, *J. Am. Chem. Soc. 123*, 11952−11959.
18. Luo, J., and Bruice, T. C. (2002) Ten-nanosecond molecular dynamics simulation of the motions of the horse liver alcohol dehydrogenase•$PhCH_2O^-$ complex, *Proc. Natl. Acad. Sci. U.S.A. 99*, 16597−16600.
19. Luo, J., and Bruice, T. C. (2004) Anticorrelated motions as a driving force in enzyme catalysis: The dehydrogenase reaction, *Proc. Natl. Acad. Sci. U.S.A. 101*, 13152−13156.
20. Kohen, A. (2006) *Isotope Effects in Chemistry and Biology*, Chapter 28, pp 743−764, CRC Press, Boca Raton, FL.
21. Cha, Y., Murray, C. J., and Klinman, J. P. (1989) Hydrogen Tunneling in Enzyme Reactions, *Science 243*, 1325−1330.
22. Liang, Z. X., Lee, T., Resing, K. A., Ahn, N. G., and Klinman, J. P. (2004) Thermal-activated protein mobility and its correlation with catalysis in thermophilic alcohol dehydrogenase, *Proc. Natl. Acad. Sci. U.S.A. 101*, 9556−9561.
23. MacBeath, G., Kast, P., and Hilvert, D. (1998) A small, thermostable, and monofunctional chorismate mutase from the archeon *Methanococcus jannaschii*, *Biochemistry 37*, 10062−10073.
24. Merz, A., Yee, M. C., Szadkowski, H., Pappenberger, G., Crameri, A., Stemmer, W. P. C., Yanofsky, C., and Kirschner, K. (2000) Improving the catalytic activity of a thermophilic enzyme at low temperatures, *Biochemistry 39*, 880−889.
25. Helmstaedt, K., Heinrich, G., Merkl, R., and Braus, G. H. (2004) Chorismate mutase of *Thermus thermophilus* is a monofunctional AroH class enzyme inhibited by tyrosine, *Arch. Microbiol. 181*, 195−203.
26. Mazumder-Shivakumar, D., Kahn, K., and Bruice, T. C. (2004) Computational study of the ground state of thermophilic indole glycerol phosphate synthase: Structural alterations at the active site with temperature, *J. Am. Chem. Soc. 126*, 5936−5937.
27. Zhang, X. H., and Bruice, T. C. (2006) Temperature Dependence of the Structure of the Substrate and Active Site of the *Thermus thermophilus* Chorismate Mutase ES Complex, *Biochemistry 45*, 8562−8567.
28. Zhang, X. H., and Bruice, T. C. (2005) The proficiency of a thermophilic chorismate mutase enzyme is solely through an entropic advantage in the enzyme reaction, *Proc. Natl. Acad. Sci. U.S.A. 102*, 18356−18360.
29. Brooks, B. R., Bruccoleri, R. E., Olafson, B. D., States, D. J., Swaminathan, S., and Karplus, M. (1983) Charmm-a Program for Macromolecular Energy, Minimization, and Dynamics Calculations, *J. Comput. Chem. 4*, 187−217.
30. Besler, B. H., Merz, K. M., and Kollman, P. A. (1990) Atomic Charges Derived from Semiempirical Methods, *J. Comput. Chem. 11*, 431−439.
31. Frisch, M. J., et al. (2004) *Gaussian 03*, Gaussian, Inc., Wallingford, CT.
32. Foloppe, N., and MacKerell, A. D. (2000) All-atom empirical force field for nucleic acids: I. Parameter optimization based on small molecule and condensed phase macromolecular target data, *J. Comput. Chem. 21*, 86−104.
33. Foloppe, N., Sagemark, J., Nordstrand, K., Berndt, K. D., and Nilsson, L. (2001) Structure, dynamics and electrostatics of the active site of glutaredoxin 3 from *Escherichia coli*: Comparison with functionally related proteins, *J. Mol. Biol. 310*, 449−470.
34. Jorgensen, W. L., Chandrasekhar, J., Madura, J. D., Impey, R. W., and Klein, M. L. (1983) Comparison of Simple Potential Functions for Simulating Liquid Water, *J. Chem. Phys. 79*, 926−935.
35. Brooks, C. L., and Karplus, M. (1989) Solvent Effects on Protein Motion and Protein Effects on Solvent Motion Dynamics of the Active-Site Region of Lysozyme, *J. Mol. Biol. 208*, 159−181.
36. Brooks, C. L., and Karplus, M. (1983) Deformable Stochastic Boundaries in Molecular-Dynamics, *J. Chem. Phys. 79*, 6312−6325.
37. Brunger, A., Brooks, C. L., and Karplus, M. (1984) Stochastic Boundary-Conditions for Molecular-Dynamics Simulations of St2 Water, *Chem. Phys. Lett. 105*, 495−500.
38. Ryckaert, J. P., Ciccotti, G., and Berendsen, H. J. C. (1977) Numerical-Integration of Cartesian Equations of Motion of a System with Constraints-Molecular-Dynamics of N-Alkanes, *J. Comput. Phys. 23*, 327−341.
39. Harte, W. E., Swaminathan, S., Mansuri, M. M., Martin, J. C., Rosenberg, I. E., and Beveridge, D. L. (1990) Domain Communication in the Dynamic Structure of Human Immunodeficiency Virus-1 Protease, *Proc. Natl. Acad. Sci. U.S.A. 87*, 8864−8868.
40. Zoete, V., Michielin, O., and Karplus, M. (2002) Relation between sequence and structure of HIV-1 protease inhibitor complexes: A model system for the analysis of protein flexibility, *J. Mol. Biol. 315*, 21−52.
41. Thorpe, I. F., and Brooks, C. L. (2005) Conformational substates modulate hydride transfer in dihydrofolate reductase, *J. Am. Chem. Soc. 127*, 12997−13006.
42. Bruice, T. C. (2002) A view at the millennium: The efficiency of enzymatic catalysis, *Acc. Chem. Res. 35*, 139−148.
43. Hu, P., and Zhang, Y. K. (2006) Catalytic mechanism and product specificity of the histone lysine methyltransferase SET7/9: An ab initio QM/MM-FE study with multiple initial structures, *J. Am. Chem. Soc. 128*, 1272−1278.
44. Benkovic, S. J., and Hammes-Schiffer, S. (2006) Biochemistry: Enzyme motions inside and out, *Science 312*, 208−209.
45. Masgrau, L., et al. (2006) Atomic description of an enzyme reaction dominated by proton tunneling, *Science 312*, 237−241.

BI062110+